Periods of Linear Development of the ENSO Cycle and POP Forecast Experiments

BENYANG TANG

School of Earth and Ocean Sciences, University of Victoria, Victoria, Canada

(Manuscript received 10 December 1991, in final form 2 May 1994)

ABSTRACT

The results of the POP (principal oscillation pattern) analysis of the tropical Pacific wind stress data are presented. The wind stress data are smoothed and detrended in the same way as that used by Lamont's coupled ocean–atmosphere model to initialize El Niño forecasts. Thus, the present wind stress POP model serves as an indicator of prediction skill of the data alone, without the use of the coupled model. The POP results show that predictions of warm and cold events can be obtained at lead times of about two seasons, which is much shorter than the lead time of more than one year achieved by Lamont's coupled ocean–atmosphere model.

It is shown that during the period of about two to three seasons before the peak of a warm/cold event, the ENSO system evolves in a linear, low-dimensional way. This property allows a precursor of a warm/cold event to be identified around May of the event year. In other periods of the ENSO cycle, the POP model does not perform well.

The author performed a cross-validation experiment, in which the data of two years following the month of the initial condition are withheld in both the EOF calculation and the POP model construction. It was found that the skill (measured by correlation coefficient) of the cross-validation model is 0.05–0.15 lower than that of the hindcast model. The ability of the cross-validation model to pick up the precursor of a warm/cold event is also slightly lower than that of the hindcast model.

1. Introduction

Among all the interannual climate variations, the El Niño–Southern Oscillation (ENSO) attracts the most attention. ENSO is primarily limited in the tropical Pacific but it also affects the global climate.

There have been many studies of ENSO forecasts [e.g., Barnett et al. (1988)]. An early ENSO forecast model by Inoue and O'Brien (1984) used a linear reduced-gravity ocean model driven by observed wind that is fixed at the model's initial time. Skillful forecasts can be made for a 3-month lead time. Graham et al. (1987) constructed two linear statistical models by canonical correlation analysis (CCA) from tropical wind stress data and sea level pressure (SLP) data, respectively. For a 3-month lead time, the model using the wind has no skill in the spring and has the best performance in November. While the model using the SLP does poorly in the least-square sense, it shows its merit in providing an El Niño warning at lead times of 7–16 months. Graham et al. (1987) also compared the performances of hindcast and cross-validation forecasts, the latter being a simulated forecast designed for removing the artificial skill of hindcast. They found that the skill of cross validation is much lower, being about the square of the hindcast skill. The first successful coupled ocean–atmosphere dynamical forecast model was constructed by a Lamont group (Cane et al. 1986; Cane 1991). The coupled model is able to forecast El Niño at lead times longer than one year with a skill of 0.6 (measured as the correlation coefficient between the observed and the modeled indices).

Recently, one statistical method, the POP (principal oscillation pattern) method, has been used to analyze ENSO dynamics (Hasselmann 1988; Xu and von Storch 1990; Latif and Flugel 1991; Blumenthal 1991). The POP methods in these studies have shown an ability of extracting oscillation information from multivariate time series. Xu and von Storch (1990) used POP to analyze the SLP data in the Pacific of 15°–40°S. They found that the method has skillful hindcasts of the ENSO system at lead times of two to three seasons. Because of the short data length, they did not do any cross validation. So the forecast skill of their model is unknown. Latif and Flugel (1991) applied the POP method to the sea level data and to the subsurface thermal structure computed from an ocean GCM. The POP patterns reveal some interesting aspects of the ENSO development and support the heat content hypothesis proposed by Wyrtki (1985) and advanced by others (e.g., Zebiak and Cane 1987; Zebiak 1989). Burger (1993) extended the method to complex principal oscillation pattern (CPOP). He showed that CPOP can model standing oscillations that the regular POP cannot resolve.

Corresponding author address: Dr. Benyang Tang, School of Earth and Ocean Sciences, University of Victoria, P.O. Box 1700, Victoria, BC V8W 2Y2, Canada.
E-mail: tang@ocean.seaoar.uvic.ca

In this study, the POP method is applied to wind stress data of the tropical Pacific. There are three motivations for this study. First, the wind stress data used here are exactly the same as the one the Lamont's coupled ocean–atmosphere model uses to initialize forecast runs (Cane et al. 1986). So, we can see how much prediction power can be achieved with the wind stress data alone, without the use of the coupled model. Our results indicate that prediction of a warm/cold event can be made at a lead time of about two seasons, which is much shorter than the lead time of more than one year achieved by Lamont's coupled ocean–atmosphere model.

Second, we want to find out when the POP model works and when it does not. While the ENSO system is a complicated one, the POP model is only a two-dimensional linear system. We certainly do not expect the two-dimensional linear POP model to have good prediction power of long lead times for all states of the system. We will show that the POP model is a good approximation in two periods (named the linear periods) of two to three seasons when an El Niño or a La Niña is developing. Thus, these two periods are more predictable by the POP model than other periods of the ENSO cycle.

Third, we compare the skills of the hindcast and cross-validation. The wind stress data we use span 24 years, long enough to allow a cross-validation experiment to estimate the forecast skill of the resulting POP model. In contrast to the finding for the CCA model by Graham et al. (1987), we found that the cross-validation model has a skill only slightly lower than that of the hindcast model.

Most ENSO studies in the literature put emphasis on the ENSO warm events, and the terms ENSO event and El Niño are interchangeable. Here, we deal with both El Niño and its opposite extreme condition, La Niña. The latter term is used less often. To avoid confusion, we use the terms warm event and cold event.

The following section describes the data and the POP calculation. Section 3 discusses the two periods of simple linear development of the ENSO cycle and identifies the event precursors. Section 4 analyzes the ENSO POP patterns to reveal what is going on during the linear development periods of the ENSO cycle. Section 5 presents results of a cross-validation experiment that estimates the forecast skill of the POP model. Section 5 also identifies precursors for possible forecasting use of the POP model. Section 6 discusses the sensitivity of the POP model.

2. POP analysis of wind stress data

a. Data

The wind stress anomaly data are derived from The Florida State University wind stress dataset (Goldenberg and O'Brien 1981). This dataset has monthly wind stress fields of 2° × 2° resolution, covering the Pacific from 29°N to 29°S, and the period from January 1961 to December 1993. The data are further processed: one pass of 1–2–1 filter is applied in longitude, latitude, and time, respectively, and the long-term trend is removed from each month by subtracting the average of the same calendar months of the previous four years. The detrend and the 1–2–1 filters act as a bandpass filter that emphasizes the variation of timescales important to the ENSO dynamics. The Lamont coupled model uses these same processed wind stress data to initialize forecasts (Cane et al. 1986).

It has been noticed (e.g., Cane et al. 1986) that the wind data before 1970 are of distinctively low quality. We thus use only the data since January 1970, which have 288 monthly wind stress fields. In section 6, where the sensitivy of the POP analysis is discussed, we will show that including the pre-1970 data decreases the hindcast skill of the POP model.

The tide gauge sea level data are from the University of Hawaii's dataset (Wyrtki 1979). The present study uses monthly sea level anomalies of 42 stations in the Pacific of 25°N–25°S. The data are used to calculate the sea level patterns associated with the wind stress POPs.

b. POP analysis of wind stress data

The POP technique used here is based on that of von Storch et al. (1988) and Latif and Flugel (1991). An empirical orthogonal function (EOF) analysis is first performed on the wind stress data $[\tau_x(t), \tau_y(t)]$, and only the first nine EOF time series $\mathbf{x}(t)$ are retained, which contain 50% of the total variance of the smoothed and detrended data. A linear model $\mathbf{A}$, which links $\mathbf{x}(t)$ and $\mathbf{x}(t+1)$, is calculated by a one-step autoregressive process to minimize the residual, so that

$$\mathbf{x}(t+1) = \mathbf{A}\mathbf{x}(t) + \text{residual}. \tag{1}$$

Eigenvectors and eigenvalues can be calculated from matrix $\mathbf{A}$. An eigenvector $\mathbf{p}_i = \mathbf{p}_i^1 + j\mathbf{p}_i^2$ is called a POP of $\mathbf{x}(t)$. The corresponding POP coefficient $z(t) = z_i^1(t) + jz_i^2(t)$ is obtained by projecting $\mathbf{x}(t)$ onto the adjoint eigenvector. Mathematically, if $\mathbf{A} = \mathbf{P}\Lambda\mathbf{P}^{-1}$, where Λ is a diagonal matrix whose elements are eigenvalues and the columns $\mathbf{p}_i$ of $\mathbf{P}$ are eigenvectors of $\mathbf{A}$, then

$$\mathbf{z}(t) = \mathbf{P}^{-1}\mathbf{x}(t).$$

The EOF time series $\mathbf{x}(t)$ can be expanded on the POP base $\mathbf{P}$; that is,

$$\mathbf{x}(t) = \mathbf{P}\mathbf{z}(t) = \text{Re}[\mathbf{P}\mathbf{z}(t)] = \sum_i [\mathbf{p}_i^1 z_i^1(t) - \mathbf{p}_i^2 z_i^2(t)]. \tag{2}$$

Upon an eigenvector transformation, the linear model Eq. (1) becomes

$$\mathbf{z}(t+1) = \Lambda\mathbf{z}(t) + \text{residual}. \tag{3}$$

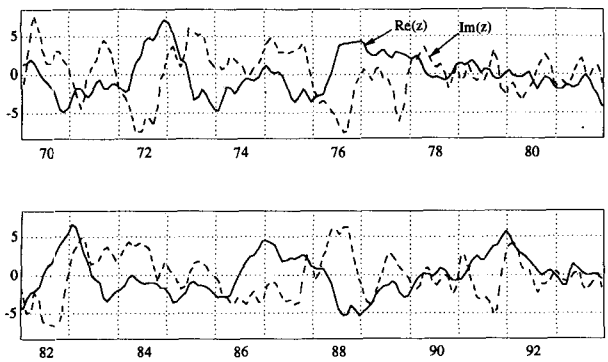

FIG. 1. The real part z^1 (solid) and the imaginary part z^2 (dashed) of the hindcast ENSO POP coefficients.

Since Λ is a diagonal matrix, each z_i is decoupled and follows a simple equation

$$z_i(t_0 + 1) = e^{-1/\tau_i} e^{j2\pi/T_i} z_i(t_0) + \text{residual}, \quad (4)$$

where T_i is the oscillation period and τ_i the e-folding decay time. From the oscillation period T_i, one can pick and study a POP of the period of one's interest.

The POP that corresponds to the complex eigenvalue of the longest decay time (11.7 months) has a period of 41 months, roughly the ENSO timescale. This POP is thus called the ENSO POP. The ENSO POP and its coefficients are denoted by $\mathbf{p}$ and $z(t)$, without the subscript i. The ENSO POP coefficients $z(t)$ contain 38% of the variance of $\mathbf{x}(t)$, so they get 50% $\times$ 38% = 19% of the total variance of the smoothed and detrended wind stress data. The real and imaginary parts $z^1(t)$ and $z^2(t)$ of the ENSO POP coefficients are plotted in Fig. 1, and the complex coefficients $z(t) = z^1(t) + jz^2(t)$ are plotted on complex planes in Fig. 2, where the horizontal and vertical axes are the real and imaginary parts of z, respectively.

In determining the ENSO POP coefficients $z(t)$, there is an arbitrary complex constant that adds a phase shift to $z(t)$. Here it was set so that in December 1982 the peak phase of a big warm event, z^1 is positive and z^2 is zero (see the 1982 plane in Fig. 2). In doing so, it is hoped that $z^1(t)$, the real part of $z(t)$, will act like an ENSO index.

Figure 3 compares z^1 with the observed NINO3 index, which is the averaged observed SST of the Pacific

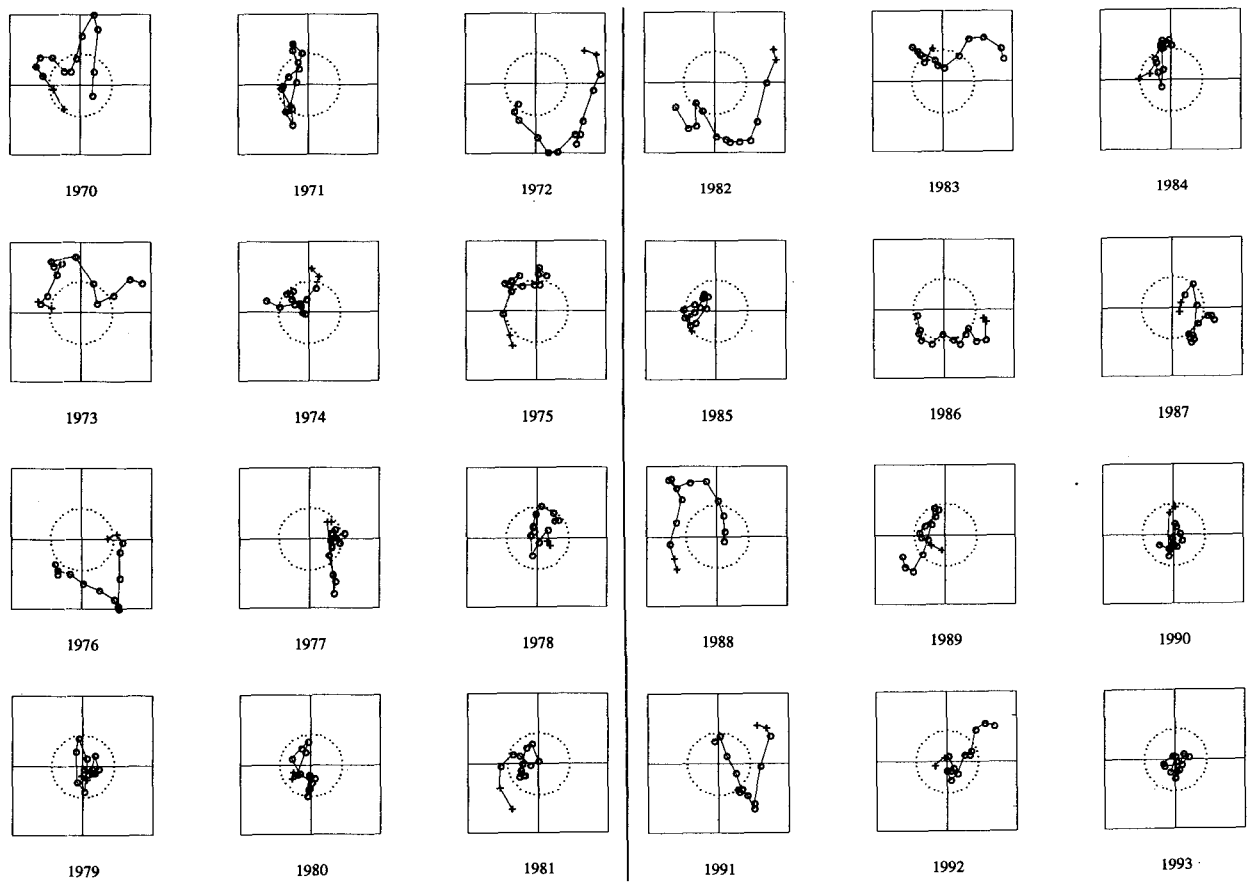

FIG. 2. Hindcast ENSO POP coefficients z are shown on complex planes. The horizontal and vertical axes represent the real and imaginary parts of z, respectively. Each plane shows the evolution of z in one year. Each "O" represents 1 month, and the two "+" in each plane are for January and February of next year. The dotted circle is $|z| = 3.42$.

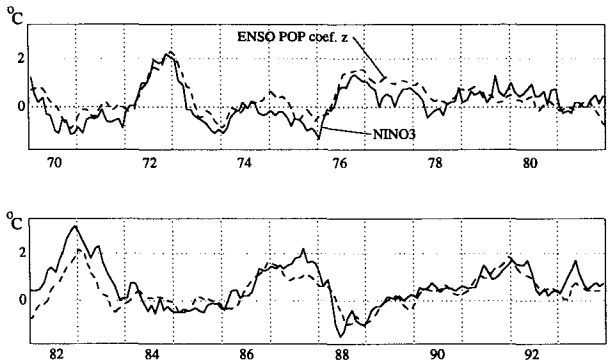

FIG. 3. Comparison of the real part z^1 of the ENSO POP coefficient and the observed NINO3. The correlation coefficient between the two is 0.76.

Ocean of 150°–90°W and 5°N–5°S and is widely used as an ENSO index. Because the NINO3 has a nonzero mean and different scale, z^1 in Fig. 3 has been transformed by a linear formula $az^1 + b$, where a and b are determined by a least-squares fit to the NINO3 index. The correlation coefficient between z^1 and NINO3 is 0.76. The term z^1 represents the five major warm events (1972, 1976, 1982, 1986, and 1991) and the five major cold events (1970, 1973, 1975, 1984, and 1988) well. However, there are many small differences between the two; the most noticeable are in 1982/83, where z^1 is smaller than NINO3, and in 1993, where z^1 does not show the short warming around March.

The correlation patterns $\mathbf{h}^1$ and $\mathbf{h}^2$ of sea level, which are associated with the wind stress ENSO POP patterns $\mathbf{p}^1$ and $\mathbf{p}^2$, respectively, can be calculated by minimizing

$$J = \|\mathbf{d}(t) - z^1(t)\mathbf{h}^1 + z^2(t)\mathbf{h}^2\|_2,$$

where $\mathbf{d}(t)$ is a vector of the monthly sea level anomalies at the tide stations, and $\|\cdot\|_2$ means a 2-norm. Solving the minimization, we get

$$\mathbf{h}^1 = [-a_{12}\langle z^2(t)\mathbf{d}(t)\rangle + a_{22}\langle z^1\mathbf{d}(t)\rangle]/(a_{11}a_{22} - a_{12}^2), \quad (5a)$$

$$\mathbf{h}^2 = [a_{12}\langle z^1(t)\mathbf{d}(t)\rangle - a_{11}\langle z^2\mathbf{d}(t)\rangle]/(a_{11}a_{22} - a_{12}^2), \quad (5b)$$

where $a_{11} = \langle z^1(t)z^1(t)\rangle$, $a_{22} = \langle z^2(t)z^2(t)\rangle$, $a_{12} = \langle z^1(t)z^2(t)\rangle$, and $\langle . \rangle$ is the average over time. The tide station data $\mathbf{d}(t)$ are very gappy, but Eq. (5) automatically excludes the contribution of the missed data when the missing data are replaced with zeros. The ENSO POP patterns $\mathbf{p}^1$ and $\mathbf{p}^2$, the real and imaginary parts of the ENSO POP, are shown in Fig. 4. Figure 5 is the associated sea level patterns $\mathbf{h}^1$ and $\mathbf{h}^2$. The patterns $\mathbf{p}^1$, $\mathbf{p}^2$, $\mathbf{h}^1$, and $\mathbf{h}^2$ are very similar to those of Latif and Flugel (1991), who did POP analysis on the sea level data and calculated the associated correlation patterns for wind stress.

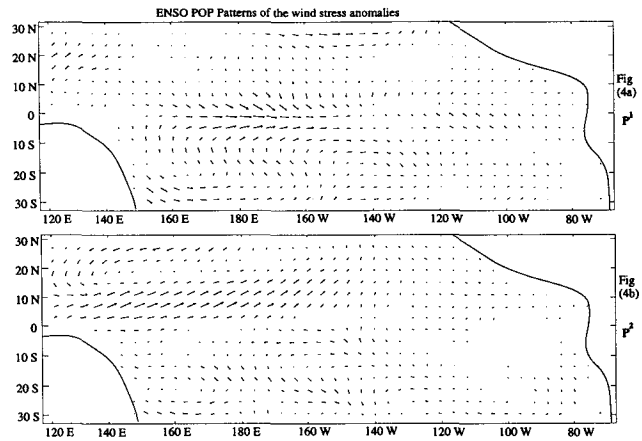

FIG. 4. Wind stress ENSO POP patterns. (a) The real part $\mathbf{p}^1$ appearing at the peak time of a warm event, and (b) the imaginary part $\mathbf{p}^2$ appearing two to three seasons before at the peak time of a warm event.

c. *A POP model and hindcast predictions*

Equation (4) divides $z(t)$ into two parts: the linear model part and the residual part. If we use Eq. (4) to model the evolution of $z(t)$, the linear part lasts roughly as long as the decay time. After that, the residual part takes over. Thus, the decay time tells how long the wind stress data fit the linear model or how long a prediction using Eq. (4) works. The decay time is also a function of filtering. More passes of 1–2–1 filter in time increase the decay time; an infinite number of passes produce time series constant in time and, thus, an infinitely long decay time. For the ENSO POP model, the decay time is ignored for the convenience of later discussions. A neutral model is assumed, and the residual is neglected. The equation for the ENSO POP becomes

$$z(t_0 + t) = e^{j2\pi t/T}z(t_0). \quad (6)$$

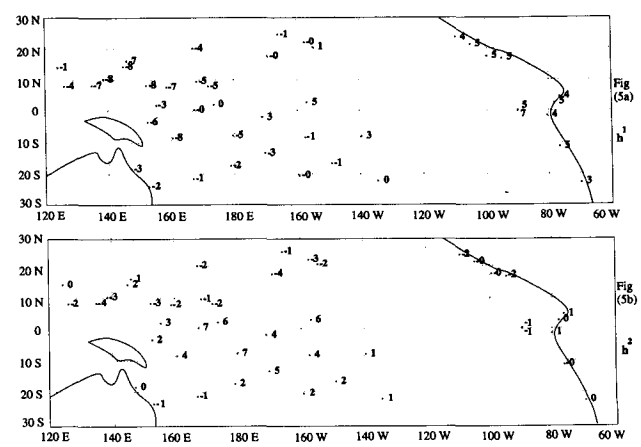

FIG. 5. The sea level patterns (a) $\mathbf{h}^1$ and (b) $\mathbf{h}^2$ associated with the wind stress patterns $\mathbf{p}^1$ and $\mathbf{p}^2$, respectively.

This is a linear model with two degrees of freedom, a great simplification from the real ENSO system.

Based on the ENSO POP model Eq. (6), a hindcast prediction z_h of the lead time t_1 is calculated:

$$z_h(t_0 + t_1) = e^{j2\pi t_1/T} z(t_0). \quad (7)$$

To see the effect of the amplitude $|z|$ on the prediction skill, we divide all the months into two groups: a quiet group, where $|z| < \langle |z| \rangle$, and a nonquiet group, where $|z| \geq \langle |z| \rangle$, the mean $\langle |z| \rangle$ being 3.42. Of all the months, 55% are in the quiet group, and 45% are in the nonquiet group.

Figure 6 shows the correlation coefficients between the hindcast prediction $z_h^1(t)$ and $z^1(t)$. Here, the time series $z^1(t)$ is used in place of observation; as seen in Fig. 3, the two are highly correlated. The correlation coefficients of the persistence prediction of z^1 are also shown as a reference. The correlation coefficient is a measure of the prediction skill, with zero as no skill and unity as perfect prediction. The correlation skill of all months is greater than 0.6 for lead times up to seven months, significantly better than the persistence skill. The skill for the nonquiet months is even higher, remaining at about 0.6 for lead times up to eight months, while the skill for the quiet group is less than persistence for lead times up to five months and considerably less than the skill for the nonquiet months. This indicates that the POP model is poor for the time when the ENSO oscillation is weak. In a study of the 30–60 day oscillation of the tropical troposphere, von Storch and Xu (1990) and von Storch and Baumhefner (1991) also found a similar dependence of prediction skill on the oscillation amplitudes.

Note that the initial condition $z(t_0)$ in Eq. (7) contains information of $t = t_0 + 1$, one month after the initial time t_0, due to the 1–2–1 filter in time applied to the original wind stress data. So the skill at a lead time of t_1 months in Fig. 6 is actually a skill of a lead time of $t_1 - 1$ months.

This prediction skill is not what we want to emphasize here; we certainly do not expect that this oversimplified system of linear evolution and two degrees of freedom can follow El Niño well all the time. As we will see in the next section, a more useful property of the ENSO POP is its ability to pick up the precursor of a warm/cold ENSO event.

3. Periods of low-dimensional linear development of the ENSO cycle

As stated in the last section, the arbitrary constant of the ENSO POP was set so that the ENSO POP coefficient $z(t)$ is a positive real number in December 1982. As a consequence, on a complex plane $z = z^1 + jz^2$ (Fig. 2), a warm event is on the positive real axis ($z^1 > 0$ and $z^2 = 0$) and a cold event is on the negative real axis ($z^1 < 0$ and $z^2 = 0$). The linear model Eq. (6) then dictates that z follows a circular motion on the complex plane; that is, z evolves in the sequence

$$\cdots \rightarrow (z^1 = 0, z^2 < 0) \rightarrow (z^1 > 0, z^2 = 0) \rightarrow (z^1 = 0, z^2 > 0) \rightarrow (z^1 < 0, z^2 = 0) \rightarrow (z^1 = 0, z^2 < 0) \rightarrow \cdots, \quad (8)$$

while the wind POP patterns appear in the sequence

$$\cdots \rightarrow \mathbf{p}^2 \rightarrow \mathbf{p}^1 \rightarrow -\mathbf{p}^2 \rightarrow -\mathbf{p}^1 \rightarrow \mathbf{p}^2 \rightarrow \cdots.$$

Each arrow represents the transition taking place in one-quarter of the oscillation period, which is $T/4 = 10.25$ months.

Sequence (8) provides a base of forecasting: detecting one phase in the sequence means the next phase will arrive in one-quarter of a period later. The forecast problem becomes the detection of the precursor state. Of course, we do not expect the states of the ENSO system to follow this simple cyclic motion at all times. A glance at Fig. 2 tells us that z is not making a circular movement in general. However, Fig. 2 does reveal that sequence (8) is almost always obeyed in two steps: $(z^1 = 0, z^2 < 0) \rightarrow (z^1 > 0, z^2 = 0)$ and $(z^1 = 0, z^2 > 0) \rightarrow (z^1 < 0, z^2 = 0)$. Here, we consider only the nonquiet months—that is, the months when $|z| > \langle |z| \rangle$ (outside the dotted circle in the complex planes of Fig. 2)—because the POP model is not as good in the quiet months (Fig. 6). In Fig. 2, the simple equation (6) works well outside of the circle $|z| > \langle |z| \rangle$ in the second quadrant ($z^1 < 0, z^2 > 0$) and the fourth quadrant ($z^1 > 0, z^2 < 0$). One can see that the step $(z^1 = 0, z^2 < 0) \rightarrow (z^1 > 0, z^2 = 0)$ was followed well in four warm event years (1972, 1976, 1982, and 1986), and the step $(z^1 = 0, z^2 > 0) \rightarrow (z^1 < 0, z^2 = 0)$ was followed well in five cold event years (1970, 1973, 1975, 1984, and 1988) (Fig. 2). A more detailed discussion will be given in section 5.

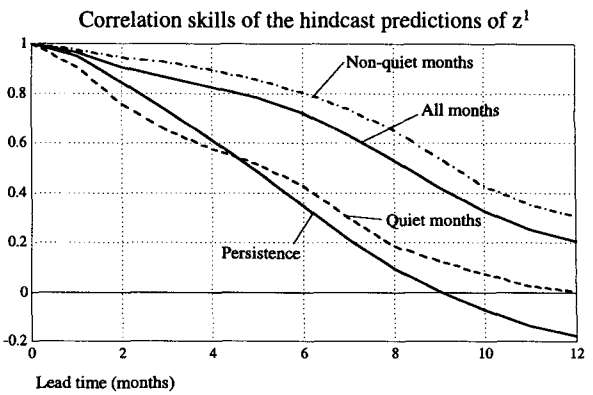

FIG. 6. The correlation skills of predicting z^1 with model Eq. (7) in the hindcast experiment. Also shown are the skills of the persistence prediction of z^1. The hindcast skills are shown in three curves: the dash–dot curve is for the nonquiet months where $|z| \geq \langle |z| \rangle$, the dashed curve is for the quiet months where $|z| < \langle |z| \rangle$, and the upper solid curve is for all months.

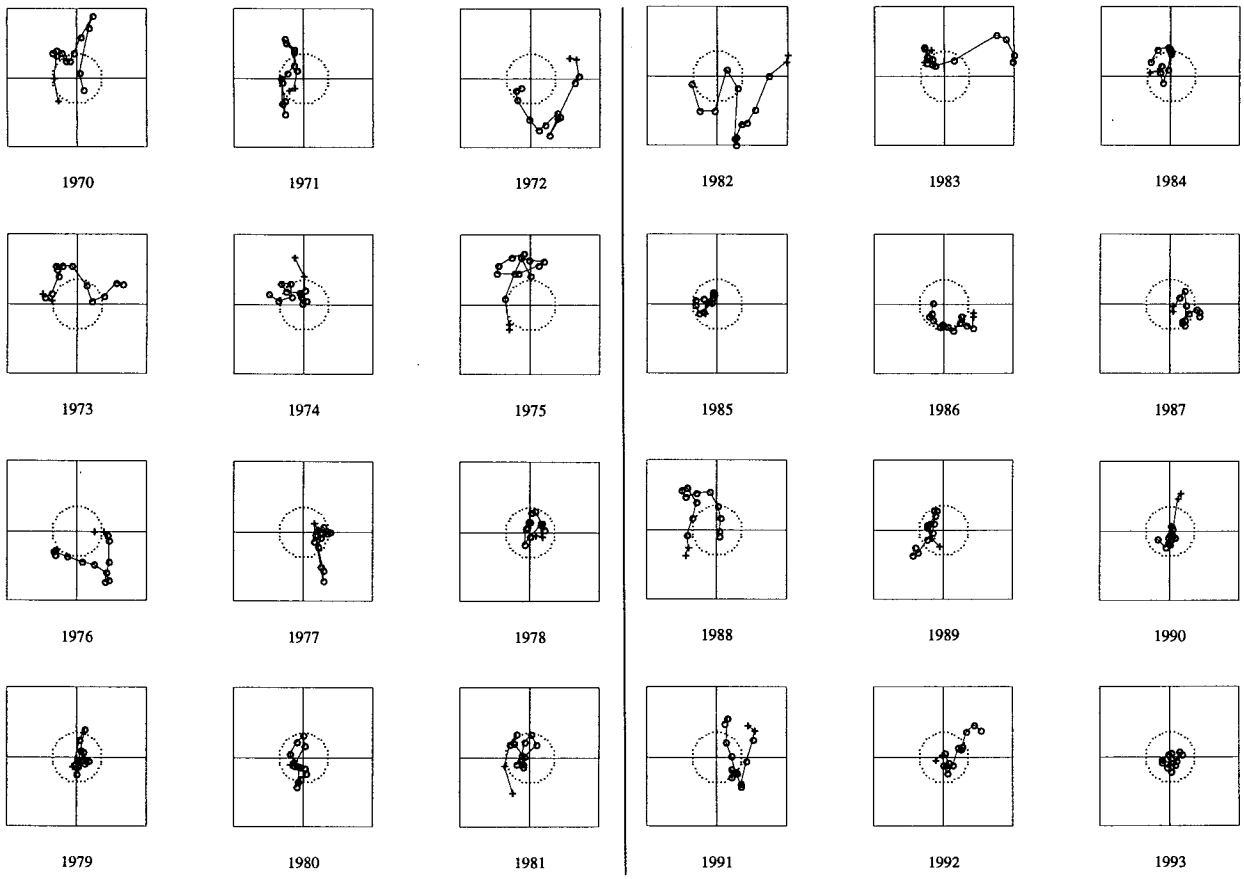

FIG. 7. ENSO POP coefficients z of cross validation are shown on complex planes. The horizontal and vertical axes represent the real and imaginary parts of z, respectively. Each plane shows the evolution of z in one year. The two "+" in each plane are for January and February of next year. The dotted circle is $|z| = 3.71$.

Thus, there appear to be two periods in the ENSO cycle when the two-dimensional linear evolution is followed for a duration of one-quarter of the cycle. The other periods of the ENSO cycle are not described well by Eq. (6) and need more complex, perhaps nonlinear, models. Fortunately, the two linear periods are the times when a forecast is most needed: a period of about two to three seasons before the peak of a warm/cold event.

4. Discussion of ENSO POP patterns

The wind stress pattern $\mathbf{p}^1$ and the associated sea level pattern $\mathbf{h}^1$ appear at the peak phase ($z^1 > 0$, $z^2 = 0$) of a warm event, while $\mathbf{p}^2$ and $\mathbf{h}^2$ appear at the precursor phase ($z^1 = 0$, $z^2 < 0$) of a warm event. In this section, we analyze the patterns and show what is going on between the two phases. The discussion below is somewhat similar to that of Zebiak (1989) and Latif and Flugel (1991), but we add some new ingredients.

At the time two to three seasons before the peak of a warm event, the wind stress anomaly, which is $\mathbf{p}^2$ (Fig. 4b), shows a strong northeastward wind stress anomaly around 10°N from 120°E to 155°W. The Ekman drift of these wind stress anomalies is consistent with the southward heat transport in the early months of a warm event year discussed by Zebiak (1989). This southward heat flux may cause the negative heat content anomalies in the northwestern Pacific and a positive heat content anomalies in and to the south of the western equatorial region seen in the associated sea level pattern $\mathbf{h}^2$ (Fig. 5b). This sea level pattern is also very similar to that obtained from a simple wind-driven ocean model of Zebiak (1989, Fig. 12a).

The pileup of warm water in the western and central equatorial Pacific around April of a warm event year, as seen in $\mathbf{h}^2$ (Fig. 5b), supports the heat content hypothesis (Wyrtki 1985). The theory proposes that before a warm event, an unstable condition is set up by the anomalous high heat content in the western Pacific, which can be readily released to the east by equatorial Kelvin waves when triggered by a westerly wind burst in the central equatorial Pacific. At the time when the pattern $\mathbf{h}^2$ appears, warm water has already accumulated in the west. Therefore, the process of piling up warm water in the western Pacific, an early stage of a

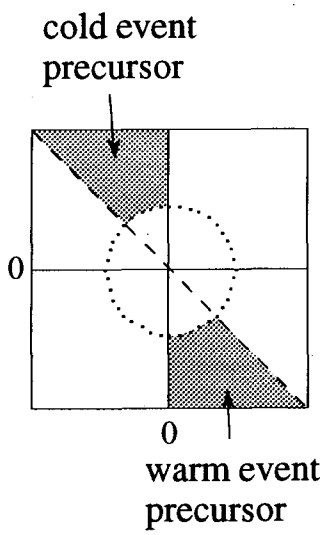

FIG. 8. Precursor areas for warm and cold events.

developing warm event, is not in the linear periods and thus is not modeled well by the simple POP model. Perhaps a major difference between the present POP model and Lamont's coupled model is the coupled model's ability of predicting the warm water accumulation.

The pattern $\mathbf{p}^1$ (Fig. 4a), appearing at the peak time of a warm event, has strong westerly anomalies around the equator east of the date line, a sign of the collapsing trade wind. The associated sea level pattern $\mathbf{h}^1$ (Fig. 5a) shows a tilt up from west to east, with minimums in the western Pacific around 10°S and 10°N. To change from $\mathbf{h}^2$ to $\mathbf{h}^1$, there must be a huge heat transport from west to east between April and December of a warm event year. Since the preevent warm water is stored mainly in the southwestern Pacific (Fig. 5b), there must also be a northward heat transport during this period at and south of the equator, as discussed by Zebiak (1989). The westerly wind patch in $\mathbf{p}^1$ is located slightly south of the equator, apparently favoring a northward heat transport. A vast area of the eastern Pacific is without any tide station, but from the positive sea level anomalies at two stations (Kanton and Christmas) around 160°W near the equator, one would reasonably guess that warm water fills the equatorial belt east of the date line, a sign of positive equatorial Kelvin waves.

As a final point on the pattern $\mathbf{h}^1$, the sea level anomalies are high in the eastern Pacific along the American coast of all latitudes up to 30° north and south; this suggests a leak of warm water from low latitudes as the positive equatorial Kelvin waves hit the eastern boundary and reflect poleward.

5. Cross-validation experiment

The analysis of the previous three sections are of the hindcast type. When the future data are unavailable, can the POP analysis still produce a precursor for the coming event? Or equivalently, what is the forecast skill of the POP model?

A cross-validation experiment, similar to that of Graham et al. (1987), was performed to estimate the forecast skill. For each month, the wind stress data of the following two years were removed, the EOF calculation and the POP analysis were done on the remaining data, and the ENSO POP coefficient and the oscillation period for the said month were calculated. These steps were repeated for every month between January 1970 and December 1993. The autocorrelation timescale of z^1 is 9 months. So the two-year windows in the cross-validation experiment should be wide enough to wipe out any influence of the data that the model attempts to predict.

Figure 7 is the resulting cross-validation ENSO POP coefficients shown on complex planes. With the similar plots for the hindcast (Fig. 2), one can compare the cross-validation model and the hindcast model in their ability of picking up the precursor of a warm/cold event. To be more quantitative, we define part of the fourth quadrant outside the circle $z = \langle |z| \rangle$ to be the precursor area of a warm event and part of the second quadrant outside the circle $z = \langle |z| \rangle$ to be the precursor area of a cold event, as indicated in Fig. 8. Whenever the ENSO POP coefficient z appears in these areas, a warm/cold event alarm is triggered.

In setting these two straightforward precursor areas, no statistical reasoning is involved. Inoue and O'Brien (1984) used sophisticated statistical procedures to set their forecast criterion. This kind of procedure should be followed to establish measures of reliability if the present POP forecasts are to be used to make decisions.

The NINO3 index in December is used as a simple criterion to classify whether a year is warm, cold, or normal. If NINO3 in December is greater than 1.0°C, the year is a warm year. If NINO3 in December is less than −0.5°C, the year is a cold year. Otherwise, the year is a normal year. This criterion is asymmetric be-

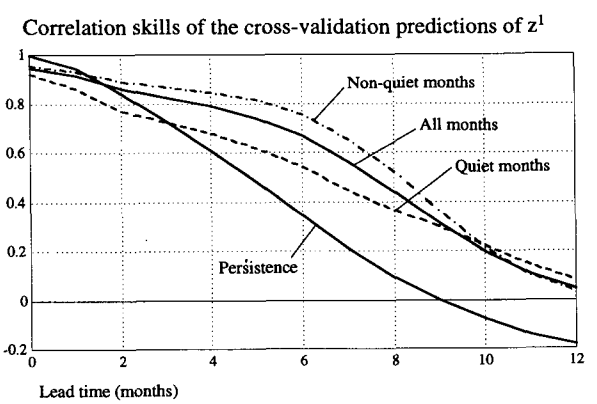

FIG. 9. The correlation skills of predicting z^1 in the cross-validation experiment. Also shown are the skills of the persistence prediction of z^1.

tween warm and cold years because warm events usually have larger amplitude than cold events, as seen in the NINO3 plot (Fig. 3). The criterion gives six warm years (1972, 1976, 1982, 1986, 1987, and 1991) and six cold years (1970, 1971, 1973, 1975, 1984, and 1988). Though the NINO3 in December 1977 is only 0.8°C, 1977 is considered here as a continued warm year, as widely recognized so. This brings the number of warm years to 7.

Table 1 lists the results of the hindcast and the cross-validation prediction of every year from 1970 to 1993. Both the hindcast and the cross validation give alarms for all the seven warm events and six cold events, although some alarms come as late as September in the event year. Of the 11 normal years, the hindcast does not issue any alarm, and the cross-validation issues two false cold alarms (1974 and 1983). In two event years (1975 and 1984), the precursor appears in the cross validation earlier than in hindcast, and in five event years (1972, 1986, 1987, 1988, and 1991), the precursor appears 1 or 2 months later than in the hindcast. Judging from the above numbers, the cross validation has a slightly lower skill than the hindcast.

Note that the above statistics depend on the somewhat arbitrary definitions of warm/cold events and the precursor areas. There were times of clear warm/cold events, but there were also times in between. The same applies to whether an alarm is triggered.

There appear to be two routes of evolution after a major warm event. The first route is the termination of the warm event. After passing the line ($z^1 > 0$ and $z^2 = 0$) outside the circle (the peak of a warm event), z enters into the first quadrant outside the circle, and the warm event does not continue into a second year. The years 1973 and 1983 and 1991 are of this route. The other route is the continued warming into the second year. After approaching the warm event line ($z^1 > 0$ and $z^2 = 0$), z goes inside the circle or turns back to the fourth quadrant, and the warm event continues for a second year. The years 1977 and 1987 are of this route. The first quadrant seems to indicate a state in which the equatorial warm water has been depleted severely and the strong warm condition cannot sustain.

It is interesting to note that the POP analysis tends to pick up the precursor of a warm/cold event around April. Many studies pointed out that April is the worst month to initiate a forecast. In a series of tests of Lamont's coupled model, three out of five failures were from April starts (Cane and Zebiak 1987). The CCA model constructed with wind stress data does poorest for April starts if the lead time is 1 month and poorest for March starts if the lead time is 3 months (Graham et al. 1987). Cane and Zebiak (1987) argued that the coupling in spring is strong and that errors in the initial condition tend to amplify fast. How the POP analysis is able to pick up a precursor in the most unstable time of the year is still not clear.

TABLE 1. The hindcast and cross-validation predictions of each year from 1970 to 1991.

			Hindcast		Cross-validation	
Year	NINO3 of Dec	Event		Month of the alarm		Month of the alarm
1970	−1.1	cold	hit	Sep	hit	Sep
1971	−0.9	cold	hit	Aug	hit	Aug
1972	2.0	warm	hit	Apr	hit	May
1973	−1.0	cold	hit	Jun	hit	Jun
1974	−0.3				false cold	Apr
1975	−1.1	cold	hit	Jun	hit	Feb
1976	1.0	warm	hit	May	hit	May
1977	0.8	warm	hit	Sep	hit	Sep
1978	0.8					
1979	0.7					
1980	0.8					
1981	0.4					
1982	3.2	warm	hit	Jun	hit	Jun
1983	0.1				false cold	Sep
1984	−0.5	cold	hit	Feb	hit	Jan
1985	−0.1					
1986	1.3	warm	hit	Jul	hit	Aug
1987	1.6	warm	hit	May	hit	Jul
1988	−1.1	cold	hit	Apr	hit	May
1989	0.2					
1990	0.5					
1991	1.5	warm	hit	May	hit	Jun
1992	0.4					
1993	0.7					
No. of warm years		7	hit 7		hit 7	
No. of cold years		6	hit 6		hit 6	
No. of normal years		11			false cold 2	

For comparison with the hindcast, we also calculated the correlation skill of the cross validation. A cross-validation prediction z_c of lead time t_1 is obtained by

$$z_c(t_0 + t_1) = e^{j2\pi t/T}\hat{z}(t_0), \qquad (9)$$

where the initial condition $z(t_0)$ is the cross-validation ENSO POP coefficient. The period T was calculated in the cross validation for each initial month t_0 and varies between 34 months and 51 months. Figure 9 shows the correlation skill of z_c^1 in predicting the hindcast ENSO POP coefficient z^1 along with the correlation skill of the persistence predictions. Compared to Fig. 6, one sees that the cross-validation skill is 0.05–0.15 lower than the hindcast skill. The skill loss in cross validation is most noticeable for the nonquiet months at lead times longer than nine months, where the difference in skill between the quiet and nonquiet months vanishes.

As in the hindcast case, the initial condition $z(t_0)$ in Eq. (9) contains information of $t = t_0 + 1$, 1 month after the initial time t_0, because of the 1–2–1 filter in time applied to the original wind stress data. So the skill at a lead time of t_1 months in Figs. 9 and 10 is actually a skill of a lead time of $(t_1 - 1)$ months.

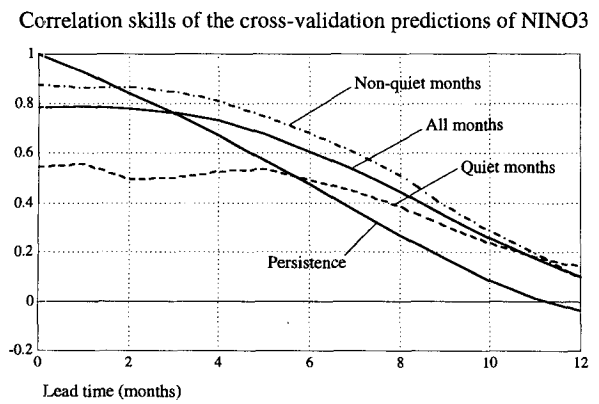

FIG. 10. The correlation skills of predicting the NINO3 index in the cross-validation experiment. Also shown are the skills of the persistence of the NINO3 index.

For comparison with other studies, we calculated the skill of using Eq. (9) to forecast NINO3. Figure 10 shows the correlation skill of z_c^1 in predicting NINO3. Comparing Figs. 9 and 10, one sees that model Eq. (9) performs only slightly poorer in predicting NINO3 than in predicting z^1; this is expected since the two quantities are correlated at 0.76 (Fig. 3). The persistence of NINO3 is 0.1–0.2 higher than that of z^1. However, model Eq. (9) still outperforms persistence at longer lead times. After the effect of the 1–2–1 filter in time is considered, the skill shown in Fig. 10 is similar to that of the POP model constructed from sea level pressure data by Xu and von Storch (1991, Fig. 7).

6. Model sensitivity

Statistical modeling is a very delicate work. There are many factors, some that matter and some that do not. Only experiments can tell which factors are important, and when they are, which values are the good choice.

In the calculation of the previous sections, only the first 9 EOFs of the wind stress data were used to build the linear model. The prediction skill deteriorates gradually when more or less EOFs are used. Figure 11 compares the hindcast skills of POP models using 7, 9, and 11 EOFs. Interestingly, in two other ENSO studies using the POP method with different datasets (Xu and Von Storch 1991; Latif and Flugel 1991), 9 EOFs were also used.

The wind stress dataset contains data back to 1961. We use only the data since 1970 because the earlier data are of poor quality as noted by Cane et al. (1986). A hindcast experiment using wind stress data back to 1964, but being tested against the same z^1 of 1970–1993, shows a slightly lower skill, as indicated in Fig. 11. With the longer data, the precursor is identified 1 or 2 months earlier but is less reliable (with more false alarms).

We fix the arbitrary complex constant of the ENSO POP by setting the ENSO POP coefficient in December 1982 to be a positive number. This automatically fixes the peak states of other warm/cold events to be around the positive/negative axis. Doing so is to clarify the relation between the precursor state and the peak state, and does not affect the skill calculation.

The POP model is constructed from the anomalies, and the annual cycle information is missing in the data. We did one experiment in which a POP model is constructed with nine EOF time series as well as a sine and a cosine time series representing the annual cycle. This resulted in a pair of additional POP modes with an exact 12-month period and an infinite decay time. The rest of the POP modes remain unchanged. The annual cycle information added in this way does not mix with anomaly data and does not play any role in the analysis. The other ways to bring in annual cycle are to build separate POP models for different seasons (Blumenthal 1991) or to use the so-called cyclostationary model as described in Hesselmann and Barnett (1981) and Johnson et al. (1985). However, these two methods increase the degrees of freedom of the model and thus decrease its generalizing ability. A nonlinear statistical model such as a neural network might be able to mix the anomaly information and the annual cycle.

The performance of the POP model depends on the method of processing the wind stress data. We use the same procedure as the one used by the forecast scheme of the Lamont's coupled model described in section 2. The detrend removes variability of periods longer than the ENSO timescale, and the 1–2–1 filter eliminates the 30–60-day oscillation, which is not resolved adequately in monthly data. Thus, the treatments emphasize the variations reasonably resolved in the data and important to ENSO dynamics.

The data processing stated above yields the best results among the following processings we have tried: the data without either time smoothing, detrending, or

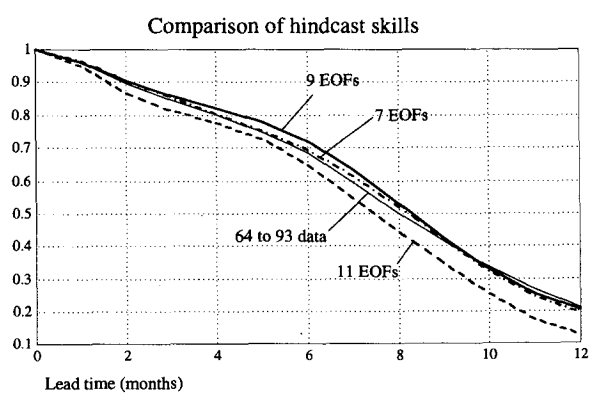

FIG. 11. Comparison of hindcast skills of POP models constructed with 7, 9, and 11 EOFs and with the 1964–1993 data. The skills are computed for all months, including quiet and nonquiet months.

both; the smoothed data detrended by a linear trend model described by Kushnir (1991); the smoothed data detrended by running means averaged from the previous 36 months of a given month. The POP model fails to pick up the ENSO signal when constructed from data without the 1–2–1 filter in time. This reveals the inability of the POP method in dealing with noisy data and the importance of temporal filtering prior to the POP analysis. The model constructed from data detrended with the 36-month running mean has almost the same correlation skill as that from our standard data processing, but the event precursors in the POP model are not as clear. Whether the 1–2–1 filter in space is performed does not affect the POP model's skill; the spatial smoothing is actually not needed because the EOF truncation has the smoothing effect as well.

Acknowledgments. I am very grateful to Dr. Mark Cane for many discussions and for his support. I also thank Drs. Steve Zebiak, Benno Blumenthal, and Yochanan Kushnir, and Ms. Yan Xue for many helpful discussions. I thank Drs. Shikiko Nakahara and Gary Mitchum for their help in getting the sea level data. This work was supported by TOGA Grant NA 87AA-D-AC081 and ONR Grant N00014-90-J1595 to Lamont-Doherty Earth Observatory of Columbia University. The revision of the work was supported by NSERC, AES, and FCAR operating grants to Andrew Weaver of the University of Victoria.

REFERENCES

Barnett, T. P., M. Graham, M. A. Cane, S. E. Zebiak, S. Dolan, J. O'Brien, and D. Legler, 1988: On the prediction of the El Niño of 1986–1987. *Science,* **241,** 192–242.

Blumenthal, M. B., 1991: Predictability of a coupled ocean–atmosphere model. *J. Climate,* **4,** 766–784.

Burger, G., 1993: Complex principal oscillation pattern analysis. *J. Climate,* **6,** 1972–1986.

Cane, M. A., 1991: Forecasting El Niño with a geophysical model. *Teleconnections Linking Worldwide Climate Anomalies,* M. Glantz, R. W. Katz, and N. Nicholls, Eds., Cambridge University Press, 155–182.

——, and S. E. Zebiak, 1987: Prediction of El Niño events using a physical model. *Atmospheric and Oceanic Variability,* H. Cattle, Ed., James Glaisher House, 153–182.

——, ——, and S. Dolan, 1986: Experimental forecasts of El Niño. *Nature,* **321,** 827–832.

Goldenberg, S. B., and J. J. O'Brien, 1981: Time and space variability of tropical Pacific wind stress. *Mon. Wea. Rev.,* **109,** 1190–1207.

Graham, N. E., J. Michaelsen, and T. P. Barnett, 1987: An investigation of the El Niño–Southern Oscillation cycle with statistical methods, 2. Model results. *J. Geophys. Res.,* **92,** 14 271–14 289.

Hasselmann, K., 1988: PIPs and POPs: The reduction of complex dynamical systems using principal interaction and oscillation patterns. *J. Geophys. Res.,* **93,** 11 015–11 021.

——, and T. P. Barnett, 1981: Techniques of linear prediction for systems with periodic statistics. *J. Atmos. Sci.,* **38,** 2275–2283.

Inoue, G. M., and J. J. O'Brien, 1984: A forecasting model for the onset of a major El Nino. *Mon. Wea. Rev.,* **112,** 2326–2337.

Johnson, C. M., P. Lemke, and T. P. Barnett, 1985: Linear prediction of sea ice anomalies. *J. Geophys. Res.,* **90,** 5665–5675.

Kushnir, Y., 1991: A simple method for the removal of the observed trend in Equatorial Pacific winds. *TOGA Notes,* No. 3, 14–16.

Latif, M., and M. Flugel, 1991: An investigation of short-range predictability in the tropical Pacific. *J. Geophys. Res.,* **96,** 2661–2674.

von Storch, H., and J. Xu, 1990: Principal oscillation pattern analysis of the 30- to 60-day oscillation in the tropical troposphere. Part I: Definition of an index and its prediction. *Climate Dyn.,* **4,** 175–190.

——, and D. P. Baumhefner, 1991: Principal oscillation pattern analysis of the tropical 30- to 60-day oscillation. Part II: The prediction of equatorial velocity potential and its skill. *Climate Dyn.,* **6,** 1–12.

——, T. Bruns, I. Fisher-Bruns, and K. H. Hasselmann, 1988: Principal oscillation pattern analysis of the 30 to 60 day oscillation in a GCM. *J. Geophys. Res.,* **93,** 11 022–11 036.

Wyrtki, K., 1979: Sea level variations: Monitoring the breath of the Pacific. *Trans Amer. Geophys. Union,* **40,** 25–27.

——, 1985: Water displacements in the Pacific and the genesis of El Nino cycles. *J. Geophys. Res.,* **4,** 7129–7132.

Xu, J.-S., and H. von Storch, 1990: Predicting the state of the Southern Oscillation using principal oscillation pattern analysis. *J. Climate,* **3,** 1316–1329.

Zebiak, S. E., 1989: Oceanic heat content variability and El Nino cycles. *J. Phys. Oceanogr.,* **19,** 475–486.

——, and M. A. Cane, 1987: A model El Nino–Southern Oscillation. *Mon. Wea. Rev.,* **115,** 2262–2278.